Drug Binding Modulates Chiral Water Structures in the DNA First Hydration Shell

Ty Santiago[1†], Daniel Konstantinovsky[1,2§†], Ethan A. Perets[1#†], Matthew Tremblay[1,3†], Sharon Hammes-Schiffer[1,3*], E. C. Y. Yan[1*]

[1]Department of Chemistry, Yale University, New Haven, CT 06520, USA

[2]Department of Molecular Biophysics and Biochemistry, Yale University, New Haven, CT 06520, USA

[3]Department of Chemistry, Princeton University, Princeton, New Jersey 08544, USA

[§]Current Address: Department of Chemistry, Columbia University, New York, New York 10027, USA

[#]Current Address: Department of Molecular Biology, University of Texas Southwestern Medical Center, Dallas, TX 75390, USA

[†]Equal Contribution

[*]Corresponding Authors; email: shs566@princeton.edu, elsa.yan@yale.edu

Abstract

Knowledge of how intermolecular interactions change hydration structures surrounding DNA will heighten understanding of DNA biology and advance drug development. However, probing changes of DNA hydration structures in response to molecular interactions and drug binding *in situ* under ambient conditions has remained challenging. Here, we apply a combined experimental and computational approach of chiral-selective vibrational sum frequency generation spectroscopy (chiral SFG) to probe changes of DNA hydration structures when a small-molecule drug, netropsin, binds the minor groove of DNA. Our results show that chiral SFG can detect water being displaced from the minor groove of DNA due to netropsin binding. The results show the promise of chiral SFG in offering mechanistic insights into roles of water in drug development targeting DNA. Our work demonstrates the power of chiral SFG to detect changes in first hydration shell structures of DNA and other biopolymers for investigating molecular mechanisms of biological processes.

Introduction

Water stabilizes DNA folding and mediates interactions of DNA with other molecules, such as proteins, small bioactive molecules, and therapeutics.[1, 2] Drugs targeting DNA molecules, such as chemotherapeutics[3, 4] and antibiotics,[5] have different binding modes, including major groove binding,[6] minor groove binding,[7] and intercalation between base pairs.[8] These binding modes differentially perturb water structures hydrating the DNA major groove, minor groove, and backbone.[9] Rational drug design targeting DNA can benefit from knowledge about these distinct perturbations to DNA hydration structures. Although structural determination techniques, such as X-ray crystallography,[10] NMR,[11] and neutron scattering techniques,[12] can provide information about hydration of DNA, they require growth of crystals, high concentration of samples, and/or low temperature, posing challenges in studying hydration in wider experimental contexts. Optical methods, on the other hand, can overcome these barriers. For example, terahertz spectroscopy can probe collective motions of water surrounding DNA,[13] Raman spectroscopy coupled with multivariate curve resolution analysis can probe hydration water,[14, 15] and two-dimensional infrared spectroscopy[16] can use site-specific vibrational probes to observe hydration structures.[17, 18] Nonlinear spectroscopic techniques including sum frequency generation (SFG)[19] and second harmonic generation[20] have also been used to probe hydration in both inorganic[21] and biological systems[20, 22] as well as biological function of biomolecules.[23] Here, we show that chiral SFG can probe perturbations of DNA hydration structures due to DNA-molecular interactions, with selectivity to water molecules in the first hydration shell of DNA.

Chiral SFG probes vibrational structures of chiral biomacromolecules,[24-29] detecting chiral macroscopic arrangements of functional groups, such as amide vibrational modes in protein secondary structures[30-32] and C-H stretches in DNA duplexes.[29, 33, 34] Chiral SFG requires a visible beam and an infrared beam to overlap to generate the second-order sum frequency signals.[35, 36] When the frequencies of the visible and SFG beams are not in resonance with an electronic transition, chiral SFG is surface specific.[26, 37, 38] Chiral SFG can even detect achiral molecules arranged in chiral supramolecular structures, thus allowing probing of vibrational structures of water molecules in hydration shells of chiral biomacromolecules.[39-41] The Petersen group showed that chiral SFG signals can detect OH stretches of water around DNA.[42] However, the origin of

the chiral water signals remained elusive. Our recent studies revealed that chiral SFG signals of water around proteins and DNA originate from water in the first hydration shells.[25, 39, 41, 43-45]

In this study, we demonstrate that chiral SFG can probe biomolecular interactions by detecting changes in water structures in the first hydration shell of double-stranded DNA (dsDNA). We study $(dA)_{12}\cdot(dT)_{12}$ dsDNA that binds an antibiotic and key drug design scaffold,[46] netropsin, in the dsDNA minor groove. We show that an increasing molar ratio of netropsin to dsDNA leads to a decrease in the chiral SFG signal of water OH stretches. Our molecular modeling reveals that the decrease of the water signals originates from displacement of water molecules from the minor groove in the first hydration shell of dsDNA due to netropsin binding. Our findings demonstrate the promise of applying chiral SFG to probe binding modes of dsDNA, including minor-groove binding, major-groove binding, and intercalation. Insights from chiral SFG can potentially inform drug development and reveal molecular mechanisms of DNA structure-function correlations. Our work also illustrates that chiral SFG can monitor structural changes in the first hydration structures of folded chiral biopolymers *in situ* under ambient conditions, offering a unique perspective for investigating biological processes.

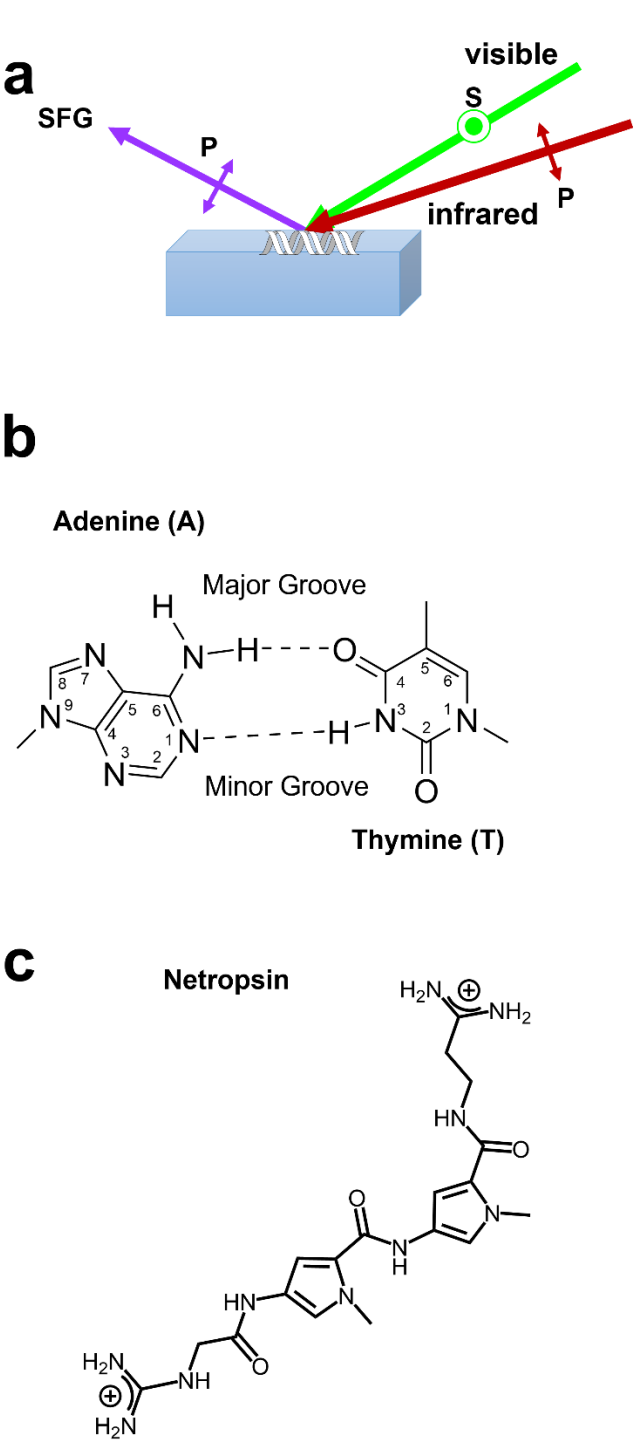

Scheme 1. (a) Chiral SFG experimental setup for probing dsDNA using an *s*-polarized visible beam and a *p*-polarized infrared beam and detecting *p*-polarized SFG signals (see Methods). (b) Adenine-thymine base pairs showing minor groove and major groove chemical moieties. (c) Chemical structure of the minor groove-binding drug netropsin.

Results

Netropsin (Scheme 1c) binds to the $(dA)_{12}\cdot(dT)_{12}$ dsDNA minor groove non-covalently and forms hydrogen bonds with adenine N3 and thymine C2=O (Scheme 1b).[47-49] Netropsin requires a minimal binding site of four adenine-thymine base pairs.[50] Thus, 2–3 netropsin molecules can bind to one $(dA)_{12}\cdot(dT)_{12}$ dsDNA. We first build fully hydrated molecular models of the $(dA)_{12}\cdot(dT)_{12}$ dsDNA bound to zero, one, and two netropsin molecules in the minor groove based on available crystal structures (see Methods). [51, 52] Our previous study shows that chiral SFG is sensitive to water molecules only in the first hydration shell of the $(dA)_{12}\cdot(dT)_{12}$ dsDNA.[44] Figure 1 (right) illustrates the molecular models with all water molecules in the first hydration shell (1st row), as well as those water molecules hydrating the minor groove (2nd row), major groove (3rd row), and backbone (4th row). Figure 1 (left) shows the corresponding simulated chiral SFG spectra of water molecules with the dsDNA binding to zero (black curve), one (red curve), and two netropsin molecules (blue curve).

The simulated chiral SFG response of water from the first hydration shell (Figure 1a) strongly depends on the number of netropsin molecules bound to the dsDNA. Binding one netropsin reduces the signal intensities by roughly one third. Binding two netropsins almost abolishes the signals. To search for the origins of these spectral changes, we dissect these responses from the first hydration shell into the responses from water molecules hydrating the minor groove (Figure 1b), major groove (Figure 1c), and the backbone (Figure 1d). Figure 1b shows that the signals from the minor groove reduce with the number of netropsin molecules. However, Figures 1c and 1d show that the signals from the major groove and backbone do not change with netropsin binding, respectively. These results suggest that the changes in the overall chiral SFG signal of water in the first hydration shell (Figure 1a) originate exclusively from the changes in hydration of the minor groove. These simulated results predict that netropsin binding displaces water molecules in the minor groove and thereby reduces the chiral SFG signals of water.

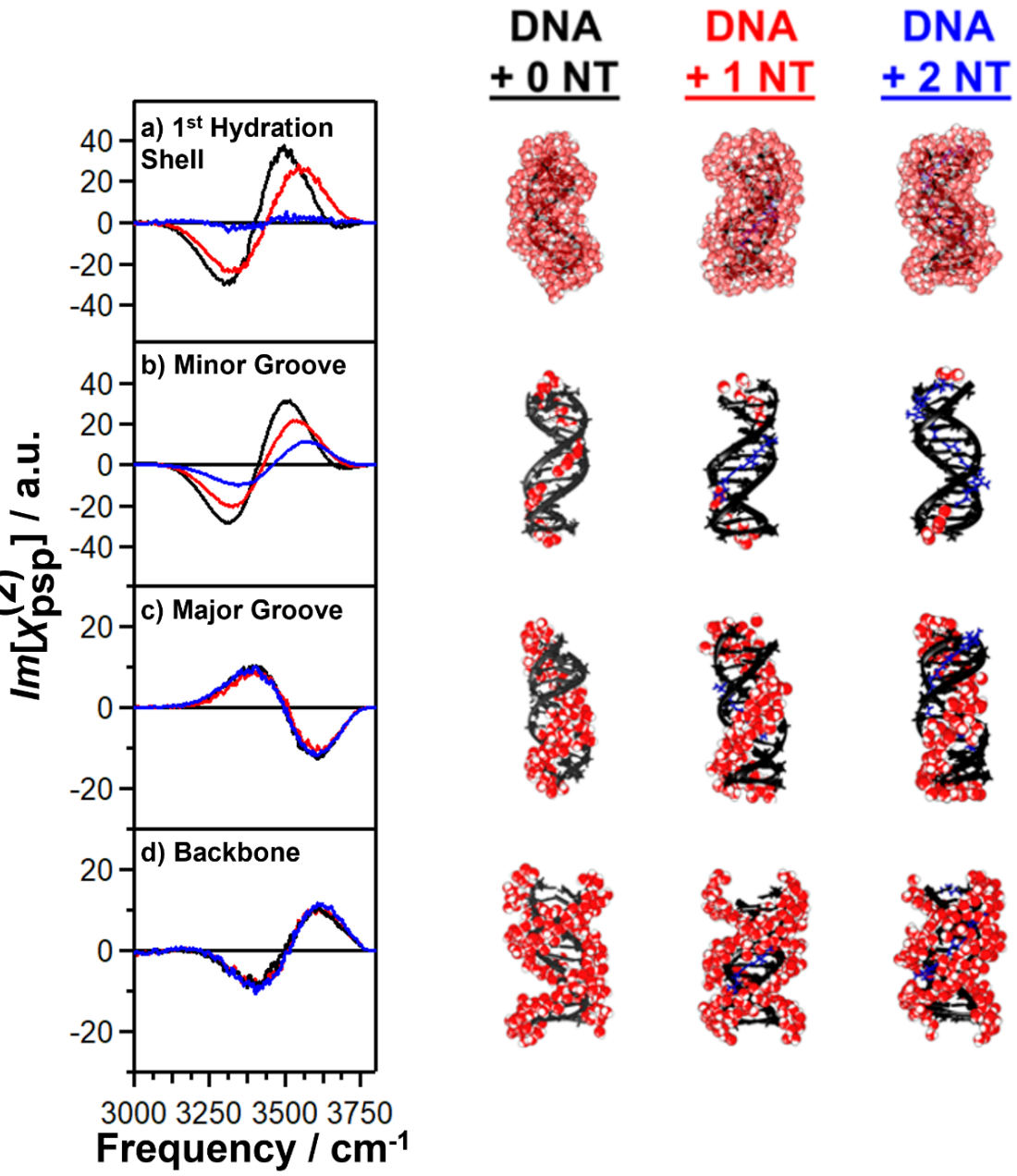

Figure 1. Simulated chiral SFG response of water and molecular models of water hydrating the $(dA)_{12}\cdot(dT)_{12}$ dsDNA bound to 0 (black), 1 (red), or 2 (blue) netropsin (NT) molecules. The simulated chiral SFG spectra (left) and molecular dynamics (MD) models (right) including hydration water and the $(dA)_{12}\cdot(dT)_{12}$ dsDNA complexed with 0, 1, or 2 netropsin molecules. (a) Water molecules in the first hydration shell and water molecules hydrating the (b) minor groove, (c) major groove, and (d) backbone. All spectra were generated by averaging over 10^6 frames from 100 ns of MD simulation. The simulated spectra contain chiral SFG responses of water but not the dsDNA. Spectral intensities are directly comparable and reported in arbitrary units (a.u.). See Methods for details on selecting the first hydration shell waters and dividing them into the subsets. The spectra and structures for DNA + 0 NT were previously reported.[44]

Guided by the computational results (Figure 1), we obtained experimental phase-resolved chiral SFG spectra of the $(dA)_{12}\cdot(dT)_{12}$ dsDNA at various molar ratios of netropsin to dsDNA, including 0:1, 1:1, 1.5:1, or 2:1 (Figure 2). Figure 2a presents the spectra (purple) and their spectral fits (black) (see the Methods section for spectral fitting procedures) with residuals of the fits (orange, top). Based on our previous studies of the $(dA)_{12}\cdot(dT)_{12}$ dsDNA hydrated in H_2O versus $H_2{}^{18}O$,[44] the global fitting includes three peaks at ~3209 cm^{-1}, ~3347 cm^{-1}, and ~3400 cm^{-1} (Figure 2b), which are assigned to NH stretches of the adenine NH_2 (Figure 2b, black curves). At the netropsin-to-DNA molar ratios of 1.5 and 2, the residual analysis suggests an additional peak at ~3510 cm^{-1} (pink) to yield satisfactory fitting. We tentatively assign this peak to an NH stretch of netropsin (Figure 2b, pink curves), as guided by our DFT calculations (see Methods and the SI). We also identified in our previous studies of the $(dA)_{12}\cdot(dT)_{12}$ dsDNA that chiral SFG signals of water contain two pairs of water OH stretches.[44] In each pair, one peak corresponds to the symmetric stretch (solid blue curves) and the other peak corresponds to the asymmetric stretch (solid red curves) (see Methods section).[44] Figure 2c shows that the first pair of water OH stretching peaks is centered at 3223 cm^{-1}, and the second pair is centered at 3503 cm^{-1}.

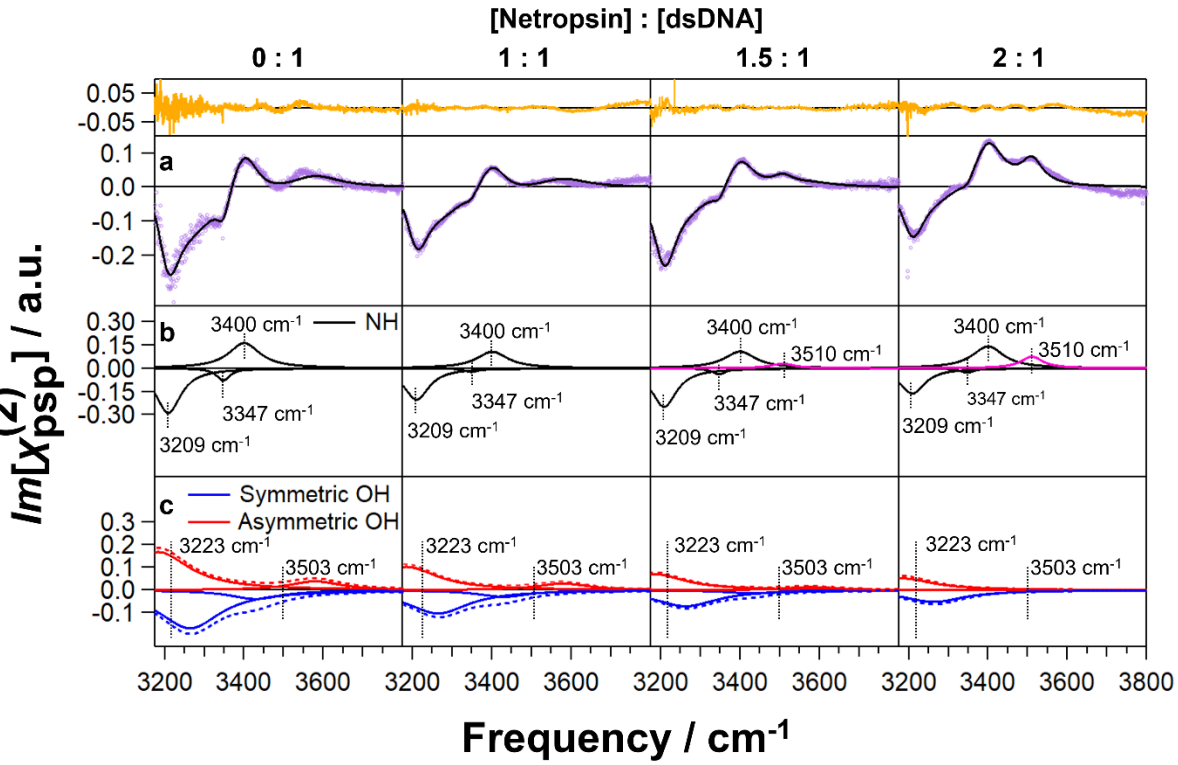

Figure 2. Experimental data and fitting of chiral SFG spectra in the OH/NH stretching region at molar ratios of netropsin:dsDNA of 0:1, 1:1, 1.5:1, and 2:1. (a) Experimental spectra (purple) and fitting curves (black) with residuals of fitting (orange, top), (b) Individual Lorentzian peaks used to fit the NH stretches from the DNA base pairs (black) and an emergent peak (pink) ascribed to NH stretches of netropsin with dotted lines marking the peak positions at 3209 cm^{-1}, 3347 cm^{-1}, 3400 cm^{-1}, and 3510 cm^{-1}, and (c) Paired symmetric (blue) and asymmetric (red) peaks from water with the solid lines showing the individual peaks and dashed lines representing the total symmetric OH stretches (blue dashed line) and the total asymmetric OH stretches (red dashed line). The first pair of water peaks is centered at 3223 cm^{-1}, and the second pair of water peaks is centered at 3503 cm^{-1}. (a.u. = arbitrary units).

Based on the fitting results, we plot the amplitude of each vibrational band as a function of the netropsin-to-DNA molar ratio (Figure 3). The amplitude is directly correlated with the molecular population because each vibrational band shares the same peak widths and peak positions across the four spectra in our global fitting (Figure 2). Figure 3 shows that the amplitudes of both water OH bands (3503 cm^{-1} and 3223 cm^{-1}) decrease with an increasing molar ratio (Figure 3a). In contrast, the amplitude of the NH stretches of dsDNA does not change significantly with the molar ratio (Figure 3b), which is consistent with the adenine NH_2 moiety pointing toward the major groove and not being perturbed by netropsin binding to the minor groove. The peak at 3510 cm^{-1} (Figure 3c) appears when the molar ratio reaches 1.5. This peak further increases at the molar

ratio of 2 (Figure 3c). We propose that this vibrational band is due to NH stretches of netropsin. Structural data show that when netropsin binds to the dsDNA, netropsin conforms to the chiral spine of the minor groove.[51, 52] This induced chiral conformation of netropsin can potentially enable the NH stretches of bound netropsin to generate chiral SFG signals.

Our analyses of experimental spectra (Figures 2 and 3) demonstrate that chiral SFG has the sensitivity for detecting changes in the hydration structures of the dsDNA due to netropsin binding. Combined with our computational modeling (Figure 1), we conclude that the experimental observations of changes in chiral SFG signals of water are due to netropsin binding that displaces water from the minor groove of the $(dA)_{12}\cdot(dT)_{12}$ dsDNA.

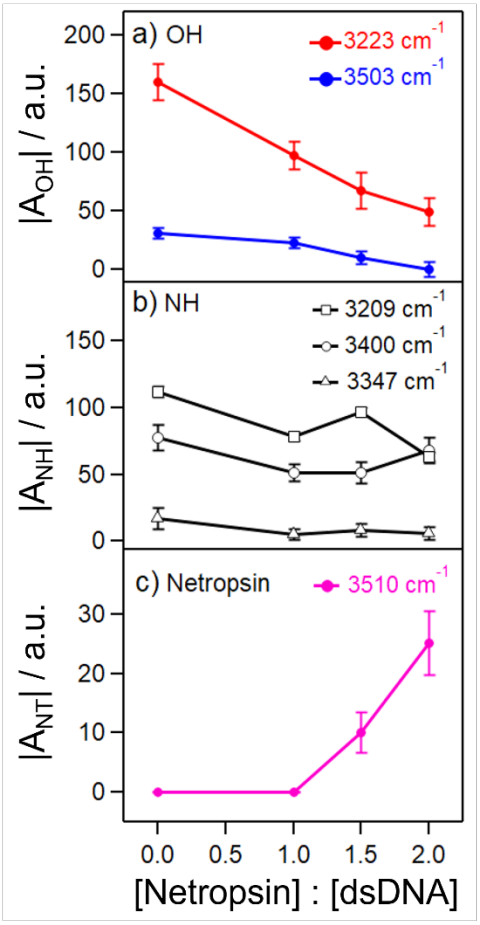

Figure 3. Changes in the amplitude of vibrational bands in the chiral SFG spectra of $(dA)_{12}\cdot(dT)_{12}$ dsDNA as a function of the molar ratio of netropsin:dsDNA: (a) the OH stretching peaks centered at 3223 cm^{-1} and 3503 cm^{-1}, (b) three peaks attributed to dsDNA NH stretches, and (c) the emergent peak at 3510 cm^{-1} ascribed to NH stretches of netropsin. (a.u. = arbitrary units)

Discussion

In our simulations, binding one molecule of netropsin to dsDNA displaces on average ~12 water molecules per frame from the dsDNA minor groove. This result agrees with previous reports that combined volumetric, calorimetric, and UV-melting measurements to estimate that ~10 water molecules are displaced from the $(dA)_{12}\cdot(dT)_{12}$ dsDNA minor groove per netropsin bound.[48] Binding a second molecule of netropsin displaces an additional ~7 water molecules from the dsDNA minor groove. Each binding event diminishes the chiral SFG response of the $(dA)_{12}\cdot(dT)_{12}$ "spine of hydration"[42, 44] by approximately one third (Figure 1b), so that dehydration of the dsDNA minor groove by netropsin progressively reduces the chiral SFG response of minor groove water molecules (Figure 1b). In stark contrast, the chiral SFG response of the major groove and phosphate backbone water subpopulations appear unaffected by netropsin binding (Figures 1c and 1d). The predicted changes in chiral SFG signals due to displacement of water from the minor groove by netropsin agree with our experimental spectra of $(dA)_{12}\cdot(dT)_{12}$ dsDNA at various netropsin:DNA molar ratios (Figure 2). Analyses of these spectra reveal that chiral SFG signals of water decrease with increasing netropsin-to-DNA molar ratios (Figure 3a).

Our residual analysis (Figure 2, top) revealed that a peak at 3510 cm^{-1} appears at the netropsin-to-DNA molar ratio of 1.5 and continues to grow at the molar ratio of 2.0 (Figure 3). This peak is unlikely to be due to hydration water as it can be fit with a single narrow Lorentzian peak.[43] The peak is also unlikely to be due to dsDNA because the DFT simulations in our previous report showed that dsDNA NH stretches of the A-T base pairs occur below 3450 cm^{-1}.[44] We propose that this peak originates from NH stretches of netropsin when bound to the $(dA)_{12}\cdot(dT)_{12}$ dsDNA minor groove, where netropsin can adopt a chiral conformation. To examine this proposition, we obtained an experimental infrared spectrum and simulated the infrared and Raman vibrational spectra of netropsin by performing DFT calculations in both implicit water and gas phase (Figure S1). The simulated spectra of netropsin show vibrational resonances from 3000 cm^{-1} to 3600 cm^{-1} due to NH stretches of netropsin. The peaks at around 3550 cm^{-1} are due to amidine stretches in the end group of the netropsin, which also appear in the experimental infrared spectrum (Figure S1c). Netropsin by itself does not produce significant chiral SFG signal (Figure S4), so

any signal that is generated when it complexes with DNA must arise from chiral induction. These computational and experimental studies support our assignment of the peak at 3510 cm^{-1} in the chiral SFG spectra (pink, Figure 2b) to netropsin.

Our experimental data reveals contributions from two pairs of OH water stretches centered at 3223 cm^{-1} and 3503 cm^{-1}. We previously identified these two OH stretching bands by globally fitting the chiral SFG spectra of the $(dA)_{12}\cdot(dT)_{12}$ dsDNA hydrated in H_2O and $H_2{}^{18}O$.[44] However, our simulated chiral SFG spectra of water hydrating the dsDNA (Figure 1a) only show a single pair of water OH stretching peaks centered at ~3400 cm^{-1} without significant signals at ~3200 cm^{-1}. The experimentally observed OH stretches at the lower frequency of 3223 cm^{-1} indicate strong H-bonding interactions of water molecules. This strong H-bonding interaction is consistent with water molecules in the minor groove forming H-bonds with the thymine C2=O group and N3 of the adenine aromatic ring (Scheme 1b). In our previous studies of protein hydration, we found that the electrostatic map used in simulating the vibrational response of water under-represents the responses from strongly H-bonded water, such as those water molecules H-bonding to the carbonyl groups of protein backbones. This issue may arise because the map was originally trained using bulk water molecules that form comparatively weak H-bonds.[53, 54] Hence, we hypothesize that our simulation of dsDNA hydration (Figure 1) may underestimate the contributions from strongly H-bonded water in the minor groove of dsDNA.

To evaluate this hypothesis, we simulated chiral SFG spectra arising from only the subset of water molecules in the minor groove of dsDNA donating a hydrogen bond to the thymine C2=O group (Figure S3a, gray curves). The lineshapes in these spectra indeed show contributions from two pairs of OH stretches centered at 3097 cm^{-1} and 3332 cm^{-1} (Figure S3c). The strongly hydrogen-bonded water molecules within this subset, corresponding to low vibrational frequencies, represent a minority within the general population of the first hydration shell. Using the current electrostatic map, the signals from these strongly hydrogen-bonded water molecules are masked by the signals from the other water molecules in the minor groove. These results suggest that expanding the training set to include water in strongly H-bonded environments in constructing the electrostatic map could potentially improve its applications to simulate vibrational responses of water in strong H-bonding environments, such as those water molecules hydrating the minor groove of dsDNA.

Intriguingly, Figure 3a shows that the lower-frequency water OH stretching band at 3223 cm^{-1} decreases to a larger extent than the high-frequency OH stretching band at 3503 cm^{-1}. Because lower OH stretching frequencies correlate with stronger H-bonding interactions, this observation suggests that strongly H-bonded water molecules are more favored to be displaced by netropsin molecules. This finding aligns with our simulation results (Figure S3) and the crystal structures of netropsin-DNA complexes reported in the literature.[51, 52] Our simulations (Figure S3a, gray curves) show that the experimentally observed low-frequency OH stretching bands at 3223 cm^{-1} are likely due to water molecules that form strong H-bonds with the thymine C2=O group (Scheme 1b) pointing to the minor groove. On the other hand, crystal structures show that netropsin binds to the minor groove of poly (dA·dT) dsDNA through forming hydrogen bonds with the adenine N3 and thymine C2=O groups (Scheme 1b).[51, 52] Thus, this structural information implies that the A-T sequence-selective binding of netropsin requires displacement of water molecules strongly H-bonded to the thymine C2=O group, in agreement with our experimental observation of a larger decrease in the intensity of the OH stretches at lower frequency (3223 cm^{-1}). As a vibrational method, chiral SFG can detect water OH stretching frequencies and thereby reveal water H-bonding interactions in the first hydration shell of folded chiral biopolymers, providing insights into sequence-selective, site-specific biomolecular interactions.

The combination of experiments and computation offers fundamental insights into how changes in dsDNA hydration upon netropsin binding correlate with spectral perturbations. Experimental chiral SFG spectra exhibit vibrational bands at various frequencies and bandwidths, which contain information about molecular structures and chemical environments. A direct comparison of simulated and experimental spectra offers quantitative assessments of the predictive power of computational approaches. Such assessments will help improve water models and develop force fields of various molecular systems for modeling important biological phenomena, such as lipid membranes interacting with biopolymers, molecular crowders impacting structures and dynamics of biopolymers,[55] and denaturants (e.g., urea) destabilizing protein structures.[56]

In this work, we demonstrate that chiral SFG can detect changes in dsDNA hydration structure resulting from minor groove binding of netropsin, a key small-molecule scaffold used in the development of drugs. We show both experimentally and computationally that increasing the concentration of netropsin depletes the chiral SFG response of water OH stretches. We also

observe an emergence of a new vibrational signal that likely originates from induced chiral organization of the drug molecule. Finally, molecular dynamics simulations and experimental chiral SFG spectra show that multiple species of water exist within the minor groove of dsDNA. These results introduce chiral SFG as a chiral-selective optical method for probing specific regions and functional groups of DNA and their interactions with other molecules *in situ*. This capability of chiral SFG to probe the interaction of biopolymers and water in the first hydration shell provides fundamental insight into the role of water in determining structure, stability, and function of the biopolymers. Thus, chiral SFG holds promises for monitoring a wide range of biological processes, offering an alternative approach for probing biological processes *in situ* by detecting changes in water structures in the first hydration shell of biopolymers, including DNA, RNA, and proteins.

Methods

Sample Preparation

Single-stranded $(dA)_{12}$ and $(dT)_{12}$ DNA oligomers were purchased from the Keck Oligonucleotide Synthesis Resource at Yale University, which were HPLC purified and used without further purification. Solutions of $(dA)_{12}\cdot(dT)_{12}$ dsDNA were prepared in water (Millipore Synergy UV-R system, 18.2 MΩ) at a concentration of 200 μM by annealing single-stranded $(dA)_{12}$ and $(dT)_{12}$ at 80 ºC for 10 minutes and allowing the solution to cool down at room temperature in a water bath. DNA solutions were then stored at 4 ºC.

Netropsin dihydrochloride (Enzo Life Sciences, ALX-380-088-M005) was procured as a lyophilized powder and prepared as a 1 mM solution in H_2O (Millipore Synergy UV-R system, 18.2 MΩ). Netropsin solution was mixed with the 200 μM $(dA)_{12}\cdot(dT)_{12}$ dsDNA and then diluted to give a final concentration of dsDNA at 100 μM and netropsin at 0 μM, 100 μM, 150 μM, or 200 μM. The mixtures were incubated at room temperature for at least one hour and were subsequently stored at 4ºC. An aliquot of 10 μL of the DNA-netropsin solutions was applied to the surface of quartz and subsequently dried in a desiccator to yield a hydrated film. We recorded the phase-resolved chiral SFG spectra of the hydrated DNA films on the surface of a right-handed z-cut α-quartz crystal (Conex Systems Technology Inc., San Jose, CA). Prior to sample preparation

the quartz was cleaned by rinsing with H_2O, dried with nitrogen, and plasma-cleaned (Harrick Plasma; PDC-32G) on "low" for 15 min.

Acquisition of phase-resolved vibrational SFG spectra

A home-built broad-bandwidth SFG spectrometer[44, 57] was used to acquire phase-resolved chiral SFG spectra of the hydrated DNA-netropsin films.[58] The *psp*-polarization (*p*-polarized sum frequency, *s*-polarized visible, *p*-polarized infrared) was used to acquire the chiral SFG spectra. Spectral frequencies were calibrated using a polystyrene reference (Buck Scientific), and cosmic rays were manually removed.[57] The spectra were recorded with the $+y$ and $-y$ axes of the quartz oriented parallel to the incident plane.[39, 59, 60] At each orientation, 10 spectra were recorded for 2 minutes. The averaged spectra were normalized to the spectrum of a clean quartz substrate. The difference between the $+y$ (I_{+y}) and $-y$ (I_{-y}) spectra yields the imaginary component of the second-order susceptibility, $Im[\chi^{(2)}]$:

$$Im[\chi^{(2)}] = \frac{(I_{+y} - I_{-y})}{4} \tag{1}$$

Analyses of experimental chiral SFG spectra

Chiral SFG signals of water contain contributions from the symmetric and asymmetric stretching modes of water in equal magnitudes but with opposite phase.[61] These two modes generate non-zero chiral SFG signal due to intramolecular coupling, yielding a unique lineshape of a doublet in opposite phases. Hence, we used the following function containing two terms to fit the chiral SFG spectra of the netropsin-DNA samples containing NH stretches of dsDNA and netropsin, and OH stretches of water:

$$f(\omega_{IR}) = Im\left[\sum_q \frac{A_q}{\omega_{IR} - \omega_q - i\Gamma_q} + \sum_n \frac{A_n}{\omega_{IR} - \left(\omega_n + \frac{1}{2}\Delta\nu_n\right) - i\Gamma_n} - \frac{A_n}{\omega_{IR} - \left(\omega_n - \frac{1}{2}\Delta\nu_n\right) - i\Gamma_n}\right] \tag{2}$$

where A_q, Γ_q, and ω_q are the amplitude, width, and vibrational frequency of the q^{th} vibrational modes other than water OH stretches; A_n and Γ_n and are the amplitude and widths of the n^{th} pair of water OH symmetric and asymmetric stretches; and $\Delta\nu_n$ and ω_n are the frequency difference and average of the n^{th} symmetric and asymmetric water OH stretches, respectively. The first term represents the independent Lorentzian peaks used to fit vibrational bands that are not associated with the chiral SFG response of water OH stretches, such as NH stretches of dsDNA and netropsin in our studies. The second term is the coupled symmetric and asymmetric stretches of water, which takes the form of a pair of positive and negative peaks of the same magnitude and width, separated from their average frequency (ω_n) by $\pm\frac{1}{2}\Delta\nu_n$.

Using Equation 2, we globally fit the chiral SFG spectra at various netropsin:dsDNA molar ratios of 0:1, 1:1, 1.5:1, and 2:1 (Figure 2). In our previous study,[44] we used Equation 2 to fit the spectrum of $(dA)_{12}\cdot(dT)_{12}$ dsDNA obtained in H_2O guided by isotopic studies using $H_2{}^{18}O$. From this previous study, we obtained the numerical values of the center peak positions (ω_n), peak widths (Γ_n), and frequency differences ($\Delta\nu_n$) for the two pairs of OH stretching bands of water, and the NH stretching frequencies (ω_q) and peak widths (Γ_q) from the $(dA)_{12}\cdot(dT)_{12}$ dsDNA spectrum acquired in H_2O in the absence of netropsin. Here, we kept the same numerical values in our global fitting of the four spectra presented in Figure 2 but let the amplitudes (A_q and A_n) of the corresponding OH stretching bands of water and NH stretching bands of the dsDNA float freely. Additionally, based on residual analysis (orange, Figure 2), we incorporated an extra Lorentzian peak in fitting the two spectra obtained at higher netropsin molar ratios (1.5:1 and 2:1). We set the position, width, and amplitude of this extra peak as free parameters in addition to the OH and NH amplitudes (A_q and A_n) in our global fitting of the four spectra shown in Figure 2 (see the SI for fitting results).

Molecular dynamics calculations

A $(dA)_{12}\cdot(dT)_{12}$ dsDNA model was constructed using the AMBER Nucleic Acid Builder.[62] To model netropsin, the RESP procedure was used to assign AMBER charge parameters, and other parameters were selected from GAFF. The DNA structure was aligned to a crystal structure of DNA with one (PDB: 6BNA)[51] or two (PDB: 358D)[52] netropsin molecules using VMD.[63] All three

systems (zero, one, and two netropsin molecules) were solvated with TIP4P-Ew water[64] and neutralized with sodium ions using AMBER's *tleap* program. Netropsin-containing systems were energy-minimized with restraints on the DNA (force constants of 500 kcal mol^{-1} $Å^{-2}$) to allow the netropsin to relax to a more favorable conformation. Following this minimization, MD simulations were carried out as described in our previous work on chiral SFG of DNA.[44] Briefly, the systems were minimized in phases with gradually loosening restraints on the DNA and netropsin until all restraints were released. The systems were then gradually heated in the NPT ensemble from 0 K to 300 K. The systems were finally equilibrated in the NPT ensemble for 5 ns and then in the NVT ensemble for 5 ps. To obtain trajectories, the system was propagated for 100 ns in the NVT ensemble, with coordinates saved every 100 fs.

Calculations of water spectra

SFG spectra of water were calculated from MD simulations using the electrostatic mapping approach developed by the Skinner lab.[54, 65-68] The inhomogeneous limit approximation was applied to the time-correlation function. Within each frame, the system was rotated such that the sixth thymine's N3-H3 bond (Scheme 1b) was aligned with the *y*-axis, with the positive direction pointing toward the hydrogen atom. The *x*-axis was chosen to point toward the thymine O2 while remaining orthogonal to the *y*-axis. Consequently, the z-axis pointed along the helical axis of the DNA, perpendicular to the base pair. Since the experimental orientation of dsDNA relative to the interface is unknown, the absolute phase of the calculated water spectra cannot be directly compared to that measured experimentally. However, the relative phases and amplitudes can be compared to experimental data. To reproduce the absolute phases observed experimentally, all calculated water spectra were multiplied by -1. For calculations involving a subset of waters, the SFG response is only a direct result of those particular waters, but all other atoms in the system also contribute to the electric field felt by each OH group within that subset.

Selection of Water Molecule Subsets

For full details of selections of the water subsets associated with the major groove, minor groove, and backbone, see our previous work on chiral SFG of dsDNA.[44] Briefly, the waters constituting the first hydration shell of dsDNA were selected by Voronoi tessellation.[45] Voronoi

tessellation divides space into regions that consist of all points that are closer to a given atom than they are to any other atom. Two atoms are defined as neighbors if the Voronoi tesserae that surround them share a face, and two molecules are defined as neighbors if any of their constituent atoms are neighbors. The first hydration shell consists of all water molecules that are neighbors of any part of the DNA, and the first hydration shell can then be divided into further subsets. Major groove water molecules were chosen as those that were closer to any atom of the major groove than to any other group in the DNA. Minor groove water molecules were chosen as those within 3.5 Å of H2 on any adenine residue. Backbone water molecules were chosen by a distance criterion analogous to that of the major groove followed by removal of water molecules near those of the minor groove to avoid contamination from the strong signal of the minor groove. For the subset of water molecules forming a strong hydrogen bond with the thymine C2=O carbonyl in the minor groove (Scheme 1b), the minor groove water selection was further filtered to select water molecules with an H_{water}-$O_{carbonyl}$ distance of 1.6 Å or less and an O_{water}-H_{water}-$O_{carbonyl}$ angle of 135° or greater. Atom selections were performed using MDAnalysis[69, 70] and in-house Python code. Voronoi tessellation was performed using the Freud library[71] to access voro++.[72]

Supporting Information

Parameters for fitting chiral SFG spectra, additional computational spectra, and experimental spectra of netropsin (PDF)

Acknowledgements

This work was supported by the NIH (R35 GM139449 to S.H.-S.) and the NSF (CHE-1905169 to E.C.Y.Y.). D.K. was supported by these grants. M.T. was supported by NIH Grant No. R35 GM139449 (S.H.-S.). E.A.P. was supported by the NIH (5T32GM008283-31) and a John C. Tully Chemistry Research Fellowship. T.S. was supported by the NSF (CHE 1905169 to E.C.Y.Y.) and the NSF MPS-Ascend Postdoctoral Research Fellowship (CHE 2402247 to T.S.). Experimental setup was supported by the NSF (CHE 2108690 to E.C.Y.Y.).

References

1. Janin, J., Wet and dry interfaces: the role of solvent in protein–protein and protein–DNA recognition. *Structure* **1999,** *7* (12), R277-R279.
2. Bischoff, G.; Hoffmann, S., DNA-binding of drugs used in medicinal therapies. *Curr. Med. Chem.* **2002,** *9* (3), 321-348.
3. Frederick, C. A.; Williams, L. D.; Ughetto, G.; Van der Marel, G. A.; Van Boom, J. H.; Rich, A.; Wang, A. H., Structural comparison of anticancer drug-DNA complexes: adriamycin and daunomycin. *Biochemistry* **1990,** *29* (10), 2538-2549.
4. Cheung-Ong, K.; Giaever, G.; Nislow, C., DNA-damaging agents in cancer chemotherapy: serendipity and chemical biology. *Chem. Biol.* **2013,** *20* (5), 648-659.
5. Finlay, A.; Hochstein, F.; Sobin, B.; Murphy, F., Netropsin, a new antibiotic produced by a Streptomyces. *J. Am. Chem. Soc.* **1951,** *73* (1), 341-343.
6. Hamilton, P. L.; Arya, D. P., Natural product DNA major groove binders. *Nat. Prod. Rep.* **2012,** *29* (2), 134-143.
7. Wemmer, D. E.; Dervan, P. B., Targeting the minor groove of DNA. *Curr. Opin. Struct. Biol.* **1997,** *7* (3), 355-361.
8. Rescifina, A.; Zagni, C.; Varrica, M. G.; Pistarà, V.; Corsaro, A., Recent advances in small organic molecules as DNA intercalating agents: Synthesis, activity, and modeling. *Eur. J. Med. Chem.* **2014,** *74*, 95-115.
9. Chalikian, T. V.; Plum, G. E.; Sarvazyan, A. P.; Breslaver, K. J., Influence of Drug Binding on DNA Hydration: Acoustic and Densimetric Characterizations of Netropsin Binding to the Poly(dAdT)·Poly(dAdT) and Poly(dA)·Poly(dT) Duplexes and the Poly(dT)·Poly(dA)·Poly(dT) Triplex at 25 °C. *Biochemistry* **1994,** *33* (29), 8629-8640.
10. Egli, M.; Tereshko, V.; Teplova, M.; Minasov, G.; Joachimiak, A.; Sanishvili, R.; Weeks, C. M.; Miller, R.; Maier, M. A.; An, H., X-ray crystallographic analysis of the hydration of A-and B-form DNA at atomic resolution. *Biopolymers: Original Research on Biomolecules* **1998,** *48* (4), 234-252.
11. Kearns, D. R.; James, T. L., NMR studies of conformational states and dynamics of DNA. *Crit. Rev. Biochem. Mol. Biol.* **1984,** *15* (3), 237-290.
12. Dahlborg, U.; Rupprecht, A., Hydration of DNA: a neutron scattering study of oriented NaDNA. *Biopolymers: Original Research on Biomolecules* **1971,** *10* (5), 849-863.
13. Plusquellic, D. F.; Siegrist, K.; Heilweil, E. J.; Esenturk, O., Applications of terahertz spectroscopy in biosystems. *ChemPhysChem* **2007,** *8* (17), 2412-2431.
14. Davis, J. G.; Rankin, B. M.; Gierszal, K. P.; Ben-Amotz, D., On the cooperative formation of non-hydrogen-bonded water at molecular hydrophobic interfaces. *Nat. Chem.* **2013,** *5* (9), 796-802.
15. Lang, X.; Shi, L.; Zhao, Z.; Min, W., Probing the structure of water in individual living cells. *Nature Communications* **2024,** *15* (1), 5271.
16. Zhang, X.-X.; Brantley, S. L.; Corcelli, S. A.; Tokmakoff, A., DNA minor-groove binder Hoechst 33258 destabilizes base-pairing adjacent to its binding site. *Comm. Biol.* **2020,** *3* (1), 525.
17. Elsaesser, T.; Schauss, J.; Kundu, A.; Fingerhut, B. P., Phosphate vibrations probe electric fields in hydrated biomolecules: spectroscopy, dynamics, and interactions. *J. Phys. Chem. B.* **2021,** *125* (15), 3899-3908.

18. Yang, M.; Szyc, Ł.; Elsaesser, T., Decelerated water dynamics and vibrational couplings of hydrated DNA mapped by two-dimensional infrared spectroscopy. *J. Phys. Chem. B* **2011,** *115* (44), 13093-13100.
19. Nihonyanagi, S.; Ishiyama, T.; Lee, T.-k.; Yamaguchi, S.; Bonn, M.; Morita, A.; Tahara, T., Unified Molecular View of the Air/Water Interface Based on Experimental and Theoretical χ(2) Spectra of an Isotopically Diluted Water Surface. *J. Am. Chem. Soc.* **2011,** *133* (42), 16875-16880.
20. Tran, R. J.; Sly, K. L.; Conboy, J. C., Applications of surface second harmonic generation in biological sensing. *Annu. Rev. Annal. Chem.* **2017,** *10* (1), 387-414.
21. Wang, H.; Chen, W.; Wagner, J. C.; Xiong, W., Local Ordering of Lattice Self-Assembled SDS@2β-CD Materials and Adsorbed Water Revealed by Vibrational Sum Frequency Generation Microscope. *J. Phys. Chem. B* **2019,** *123* (29), 6212-6221.
22. Chen, X.; Hua, W.; Huang, Z.; Allen, H. C., Interfacial Water Structure Associated with Phospholipid Membranes Studied by Phase-Sensitive Vibrational Sum Frequency Generation Spectroscopy. *J. Am. Chem. Soc.* **2010,** *132* (32), 11336-11342.
23. Okur, H. I.; Hladílková, J.; Rembert, K. B.; Cho, Y.; Heyda, J.; Dzubiella, J.; Cremer, P. S.; Jungwirth, P., Beyond the Hofmeister Series: Ion-Specific Effects on Proteins and Their Biological Functions. *J. Phys. Chem. B* **2017,** *121* (9), 1997-2014.
24. Yan, E. C. Y.; Wang, Z.; Fu, L., Proteins at interfaces probed by chiral vibrational sum frequency generation spectroscopy. *J. Phys. Chem. B* **2015,** *119* (7), 2769-2785.
25. Yan, E. C. Y.; Perets, E. A.; Konstantinovsky, D.; Hammes-Schiffer, S., Detecting Interplay of Chirality, Water, and Interfaces for Elucidating Biological Functions. *Acc. Chem. Res.* **2023**, 22421-22426.
26. Yan, E. C. Y.; Fu, L.; Wang, Z.; Liu, W., Biological macromolecules at interfaces probed by chiral vibrational sum frequency generation spectroscopy. *Chem. Rev.* **2014,** *114* (17), 8471-8498.
27. Wang, J.; Chen, X.; Clarke, M. L.; Chen, Z., Detection of chiral sum frequency generation vibrational spectra of proteins and peptides at interfaces in situ. *Proc. Nat. Acad. Sci.* **2005,** *102* (14), 4978-4983.
28. Hosseinpour, S.; Roeters, S. J.; Bonn, M.; Peukert, W.; Woutersen, S.; Weidner, T., Structure and dynamics of interfacial peptides and proteins from vibrational sum-frequency generation spectroscopy. *Chem. Rev.* **2020,** *120* (7), 3420-3465.
29. Stokes, G. Y.; Gibbs-Davis, J. M.; Boman, F. C.; Stepp, B. R.; Condie, A. G.; Nguyen, S. T.; Geiger, F. M., Making "sense" of DNA. *J. Am. Chem. Soc.* **2007,** *129* (24), 7492-7493.
30. Fu, L.; Liu, J.; Yan, E. C. Y., Chiral sum frequency generation spectroscopy for characterizing protein secondary structures at interfaces. *J. Am. Chem. Soc.* **2011,** *133* (21), 8094-8097.
31. Fu, L.; Ma, G.; Yan, E. C. Y., In situ misfolding of human islet amyloid polypeptide at interfaces probed by vibrational sum frequency generation. *J. Am. Chem. Soc.* **2010,** *132* (15), 5405-5412.
32. Zhang, B.; Tan, J.; Li, C.; Zhang, J.; Ye, S., Amide I SFG spectral line width probes the lipid–peptide and peptide–peptide interactions at cell membrane in situ and in real time. *Langmuir* **2018,** *34* (25), 7554-7560.
33. Perets, E. A.; Olesen, K. B.; Yan, E. C. Y., Chiral Sum Frequency Generation Spectroscopy Detects Double-Helix DNA at Interfaces. *Langmuir* **2022,** *38* (18), 5765-5778.

34. Walter, S. R.; Geiger, F. M., DNA on stage: showcasing oligonucleotides at surfaces and interfaces with second harmonic and vibrational sum frequency generation. *J. Am. Chem. Soc.* **2010,** *1* (1), 9-15.
35. Shen, Y. R., Surface properties probed by second-harmonic and sum-frequency generation. *Nat.* **1989,** *337* (6207), 519-525.
36. Wang, H.-F., Sum frequency generation vibrational spectroscopy (SFG-VS) for complex molecular surfaces and interfaces: Spectral lineshape measurement and analysis plus some controversial issues. *Prog. Surf. Sci.* **2016,** *91* (4), 155-182.
37. Moad, A. J.; Simpson, G. J., A unified treatment of selection rules and symmetry relations for sum-frequency and second harmonic spectroscopies. *J. Phys. Chem. B* **2004,** *108* (11), 3548-3562.
38. Simpson, G. J., Molecular origins of the remarkable chiral sensitivity of second-order nonlinear optics. *ChemPhysChem* **2004,** *5* (9), 1301-1310.
39. Perets, E. A.; Konstantinovsky, D.; Fu, L.; Chen, J.; Wang, H.-F.; Hammes-Schiffer, S.; Yan, E. C. Y., Mirror-image antiparallel β-sheets organize water molecules into superstructures of opposite chirality. *Proc. Nat. Acad. Sci.* **2020,** *117* (52), 32902-32909.
40. Perets, E. A.; Yan, E. C. Y., The H2O Helix: The Chiral Water Superstructure Surrounding DNA. *ACS Cent. Sci.* **2017,** *3* (7), 683-685.
41. Konstantinovsky, D.; Perets, E. A.; Santiago, T.; Velarde, L.; Hammes-Schiffer, S.; Yan, E. C. Y., Detecting the first hydration shell structure around biomolecules at interfaces. *ACS Cent. Sci.* **2022,** *8* (10), 1404-1414.
42. McDermott, M. L.; Vanselous, H.; Corcelli, S. A.; Petersen, P. B., DNA's chiral spine of hydration. *ACS Cent. Sci.* **2017,** *3* (7), 708-714.
43. Konstantinovsky, D.; Santiago, T.; Tremblay, M.; Simpson, G. J.; Hammes-Schiffer, S.; Yan, E. C. Y., Theoretical basis for interpreting heterodyne chirality-selective sum frequency generation spectra of water. *J. Chem. Phys.* **2024,** *160* (5).
44. Perets, E. A.; Konstantinovsky, D.; Santiago, T.; Videla, P. E.; Tremblay, M.; Velarde, L.; Batista, V. S.; Hammes-Schiffer, S.; Yan, E. C. Y., Beyond the "spine of hydration": Chiral SFG spectroscopy detects DNA first hydration shell and base pair structures. *J. Chem. Phys.* **2024,** *161* (9).
45. Konstantinovsky, D.; Yan, E. C. Y.; Hammes-Schiffer, S., Characterizing interfaces by Voronoi tessellation. *J. Chem. Phys. Lett.* **2023,** *14* (23), 5260-5266.
46. Suckling, C. J.; Hunter, I. S.; Scott, F. J., Multitargeted anti-infective drugs: resilience to resistance in the antimicrobial resistance era. *Future Drug Discov* **2022,** *4* (1), Fdd73.
47. Burckhardt, G.; Votavova, H.; Sponar, J.; Luck, G.; Zimmer, C., Two binding modes of netropsin are involved in the complex formation with poly(dA-dT).poly(dA-dT) and other alternating DNA duplex polymers. *J. Biomol. Struct. Dyn.* **1985,** *2* (4), 721-36.
48. Marky, L. A.; Kupke, D. W., Probing the hydration of the minor groove of A:T synthetic DNA polymers by volume and heat changes. *Biochemistry* **1989,** *28* (26), 9982-9988.
49. Degtyareva, N. N.; Wallace, B. D.; Bryant, A. R.; Loo, K. M.; Petty, J. T., Hydration changes accompanying the binding of minor groove ligands with DNA. *Biophys. J.* **2007,** *92* (3), 959-65.
50. Zimmer, C.; Luck, G.; Fric, I., Duplex structure formation between oligo(dA)'s and oligo(dT)'s generated by thymine-specific interaction with netropsin. *Nucleic Acids Res.* **1976,** *3* (6), 1521-32.

51. Kopka, M. L.; Yoon, C.; Goodsell, D.; Pjura, P.; Dickerson, R. E., Binding of an antitumor drug to DNA, Netropsin and C-G-C-G-A-A-T-T-BrC-G-C-G. *J. Mol. Biol.* **1985,** *183* (4), 553-63.
52. Chen, X.; Mitra, S. N.; Rao, S. T.; Sekar, K.; Sundaralingam, M., A novel end-to-end binding of two netropsins to the DNA decamers d(CCCCCIIIII)2, d(CCCBr5CCIIIII)2and d(CBr5CCCCIIIII)2. *Nucleic Acids Res.* **1998,** *26* (23), 5464-71.
53. Pieniazek, P. A.; Tainter, C. J.; Skinner, J. L., Interpretation of the water surface vibrational sum-frequency spectrum. *J. Chem. Phys.* **2011,** *135* (4).
54. Auer, B.; Skinner, J., Vibrational sum-frequency spectroscopy of the water liquid/vapor interface. *J. Phys. Chem. B* **2009,** *113* (13), 4125-4130.
55. Harada, R.; Sugita, Y.; Feig, M., Protein crowding affects hydration structure and dynamics. *J. Am. Chem. Soc.* **2012,** *134* (10), 4842-4849.
56. Ganguly, P.; Polák, J.; van der Vegt, N. F.; Heyda, J.; Shea, J.-E., Protein stability in TMAO and mixed urea–TMAO solutions. *J. Phys. Chem. B* **2020,** *124* (29), 6181-6197.
57. Ma, G.; Liu, J.; Fu, L.; Yan, E. C., Probing water and biomolecules at the air–water interface with a broad bandwidth vibrational sum frequency generation spectrometer from 3800 to 900 cm− 1. *Appl. Spectrosc.* **2009,** *63* (5), 528-537.
58. Konstantinovsky, D.; Perets, E. A.; Santiago, T.; Olesen, K.; Wang, Z.; Soudackov, A. V.; Yan, E. C. Y.; Hammes-Schiffer, S., Design of an Electrostatic Frequency Map for the NH Stretch of the Protein Backbone and Application to Chiral Sum Frequency Generation Spectroscopy. *J. Phys. Chem. B* **2023,** *127* (11), 2418-2429.
59. Ji, N.; Ostroverkhov, V.; Chen, C.-Y.; Shen, Y.-R., Phase-sensitive sum-frequency vibrational spectroscopy and its application to studies of interfacial alkyl chains. *J. Am. Chem. Soc.* **2007,** *129* (33), 10056-10057.
60. Fu, L.; Chen, S.-L.; Wang, H.-F., Validation of Spectra and Phase in Sub-1 cm-1 Resolution Sum-Frequency Generation Vibrational Spectroscopy through Internal Heterodyne Phase-Resolved Measurement. *J. Phys. Chem. B* **2016,** *120* (8), 1579-1589.
61. Konstantinovsky, D.; Perets, E. A.; Yan, E. C. Y.; Hammes-Schiffer, S., Simulation of the Chiral Sum Frequency Generation Response of Supramolecular Structures Requires Vibrational Couplings. *J. Phys. Chem. B* **2021,** *125* (43), 12072-12081.
62. Case, D. A.; Aktulga, H. M.; Belfon, K.; Cerutti, D. S.; Cisneros, G. A.; Cruzeiro, V. W. D.; Forouzesh, N.; Giese, T. J.; Götz, A. W.; Gohlke, H., AmberTools. *J. Chem. Inf. Model.* **2023,** *63* (20), 6183-6191.
63. Humphrey, W.; Dalke, A.; Schulten, K., VMD: visual molecular dynamics. *J. Mol. Graphics Modell.* **1996,** *14* (1), 33-38.
64. Horn, H. W.; Swope, W. C.; Pitera, J. W.; Madura, J. D.; Dick, T. J.; Hura, G. L.; Head-Gordon, T., Development of an improved four-site water model for biomolecular simulations: TIP4P-Ew. *J. Chem. Phys.* **2004,** *120* (20), 9665-9678.
65. Auer, B.; Skinner, J., Dynamical effects in line shapes for coupled chromophores: Time-averaging approximation. *J. Chem. Phys.* **2007,** *127* (10).
66. Pieniazek, P.; Tainter, C.; Skinner, J., Interpretation of the water surface vibrational sum-frequency spectrum. *J. Chem. Phys.* **2011,** *135* (4).
67. Auer, B.; Skinner, J., IR and Raman spectra of liquid water: Theory and interpretation. *J. Chem. Phys.* **2008,** *128* (22).

68. Corcelli, S.; Lawrence, C.; Skinner, J., Combined electronic structure/molecular dynamics approach for ultrafast infrared spectroscopy of dilute HOD in liquid H2O and D2O. *J. Chem. Phys.* **2004,** *120* (17), 8107-8117.
69. Michaud-Agrawal, N.; Denning, E. J.; Woolf, T. B.; Beckstein, O., MDAnalysis: a toolkit for the analysis of molecular dynamics simulations. *J. Comput. Chem.* **2011,** *32* (10), 2319-2327.
70. Gowers, R. J.; Linke, M.; Barnoud, J.; Reddy, T. J. E.; Melo, M. N.; Seyler, S. L.; Domanski, J.; Dotson, D. L.; Buchoux, S.; Kenney, I. M. *MDAnalysis: a Python package for the rapid analysis of molecular dynamics simulations*; 2575-9752; Los Alamos National Laboratory (LANL), Los Alamos, NM (United States): 2019.
71. Ramasubramani, V.; Dice, B. D.; Harper, E. S.; Spellings, M. P.; Anderson, J. A.; Glotzer, S. C., freud: A software suite for high throughput analysis of particle simulation data. *Comput. Phys. Commun.* **2020,** *254*, 107275.
72. Rycroft, C. H., VORO plus plus: A three-dimensional Voronoi cell library in C plus. *Chaos* **2009,** *19* (4).

For table of contents only